Schisandrin B suppresses cholangiocarcinoma by targeting the ROS/p38 MAPK/NF-κB axis

JUNHAO YANG[1*], WENYING LONG[2*], XIAOXIAO WU[3], XIAOHUI YANG[1], QIANG HONG[1] and SHUAI WANG[1]

[1]Department of General Surgery, The Fourth Affiliated Hospital of School of Medicine, and International School of Medicine, International Institutes of Medicine, Zhejiang University, Yiwu, Zhejiang 322000, P.R. China; [2]Department of Medical Research Center, Fourth Affiliated Hospital, Zhejiang University School of Medicine, Yiwu, Zhejiang 322000, P.R. China; [3]Department of Endocrinology, Yiwu Central Hospital, Yiwu, Zhejiang 322000, P.R. China

Received November 4, 2025; Accepted February 27, 2026

DOI: 10.3892/ol.2026.15551

Abstract. Schisandrin B (Sch B), a bioactive component isolated from the traditional Chinese medicine Schisandra chinensis, exhibits anti-tumor activity against cholangiocarcinoma (CCA), though its complete molecular mechanism remains to be fully elucidated. The present study employed an integrated strategy combining network pharmacology for target prediction, molecular docking for binding affinity validation and comprehensive *in vitro* experiments to investigate the regulation of the reactive oxygen species (ROS)/p38MAPK/NF-κB signaling axis by Sch B. Computational analyses revealed significant enrichment of Sch B targets in cancer-related pathways and MAPK signaling, while molecular docking confirmed strong binding to core targets including MAPK1. Experimental validation demonstrated that Sch B dose-dependently elevated intracellular ROS levels, resulting in suppressed proliferation and induced apoptosis in CCA cells, effects reversible by the ROS scavenger N-acetyl-L-cysteine. Mechanistic studies further identified that Sch B concurrently inhibits p38 MAPK signaling through reduced phosphorylated-p38 and AP-1 expression, and suppresses NF-κB pathway activation by impeding p65 nuclear translocation, leading to diminished release of pro-inflammatory cytokines IL-6, IL-8 and TNF-α. These findings collectively establish that Sch B exerts its anti-CCA effects through ROS-mediated coordinated regulation of both p38MAPK and NF-κB pathways, underscoring its potential as a multi-target natural therapeutic agent for CCA treatment and providing a solid foundation for further development.

Correspondence to: Dr Shuai Wang, Department of General Surgery, The Fourth Affiliated Hospital of School of Medicine, and International School of Medicine, International Institutes of Medicine, Zhejiang University, N1 Shangcheng Road, Yiwu, Zhejiang 322000, P.R. China
E-mail: 8011020@zju.edu.cn

*Contributed equally

Key words: Schisandrin B, cholangiocarcinoma, ROS/p38MAPK/NF-κB, network pharmacology, molecular docking

Introduction

Cholangiocarcinoma (CCA), the second most prevalent primary hepatic malignancy originating from bile duct epithelial cells, accounts for ~15% of all primary liver tumors, with a rising global incidence and mortality (1,2). It is characterized by pronounced pro-fibroplasia, a complex tumor microenvironment, and considerable genetic heterogeneity, all contributing to heightened drug resistance. Non-specific clinical manifestations often lead to delayed diagnoses, precluding timely surgical interventions and resulting in an unfavorable prognosis. Epidemiological data highlight an increasing incidence and mortality, with CCA accounting for 15% of liver malignancies (3-5). Consequently, there is an urgent need to elucidate novel strategies and pharmacological interventions to counteract CCA tumor metastasis and combat chemotherapy resistance.

Schisandrin B (Sch B), derived from the fruit of Schisandra chinensis Baill and used in traditional Chinese medicine, has demonstrated therapeutic efficacy across various malignant tumors, including glioma (6,7), gallbladder cancer (8), breast cancer (9), prostate cancer (10) and hepatic cancer (11), by eliciting anti-proliferative and pro-apoptotic effects. Previous research has indicated mitochondria-mediated intrinsic apoptotic pathways as one of its validated biological mechanisms.

Reactive oxygen species (ROS), byproducts of aerobic metabolism, play a key role in physiological processes and REDOX balance maintenance (12-14). ROS act as initiators and mediators of multiple signal transduction pathways, exerting inhibitory effects on tumor cell proliferation. They are involved in mediating various anti-tumorigenic signaling pathways inducing DNA damage, genetic instability and oxidative stress-associated tumor cell apoptosis (15). Mounting evidence has established that the ROS-activated mitochondria-mediated intrinsic apoptosis pathway represents a central mechanism underlying these effects (16-18). Mitochondria, the main site of

oxygen-free radical production, undergo alterations in permeability with increased ROS leading to decreased mitochondrial transmembrane potential ($\Delta\Psi m$). The resulting decrease in $\Delta\Psi m$ facilitates the release of cytochrome *c* into the cytoplasm, initiating apoptosis via the caspase pathway (19).

Network pharmacology enables comprehensive target-based functional analysis and prediction of drug components and diseases, thus providing a robust framework for elucidating the complex mechanisms of drug action and disease pathology (20-22). The present study was designed to investigate the anti-CCA mechanism of Sch B using an integrated strategy combining network pharmacology, molecular docking and *in vitro* experiments, with a focus on the ROS/p38 MAPK/NF-κB signaling pathway. This multi-faceted approach may provide a foundation for understanding the therapeutic potential of Sch B as a natural-derived agent against CCA.

Materials and methods

Network pharmacology. Potential targets of Sch B were predicted using the PharmMapper database (http://www.lilab-ecust.cn/pharmmapper/), followed by standardization via the UniProt database (https://www.uniprot.org/) to obtain relevant target information. Disease-related targets for CCA were retrieved from the GeneCards (https://www.genecards.org/) and DisGeNET databases (https://www.disgenet.org/) using the keyword 'Cholangiocarcinoma'. After merging datasets, non-human genes and duplicate entries were removed to generate a standardized target list. An EVenn online tool (http://www.ehbio.com/test/venn) was employed to construct a Venn diagram illustrating overlapping targets between Sch B and CCA.

The shared targets were imported into the STRING database (https://string-db.org/) to construct a protein-protein interaction (PPI) network under the 'Homo sapiens' setting. Disconnected nodes were hidden, and a high confidence interaction score of ≥0.900 was applied. The resulting network was exported in Tab-Separated Values format and visualized using Cytoscape 3.8.0 (https://cytoscape.org/). Core targets are identified based on three topological parameters: Degree centrality (DC), betweenness centrality (BC) and closeness centrality (CC).

The drug-disease intersection targets were uploaded to the Metascape platform (http://metascape.org/) for gene ontology (GO) (https://geneontology.org/) enrichment analysis, including biological process (BP), cellular component and molecular function (MF) categories. Analysis parameters included a minimum overlap of 3, a P-value cut-off of 0.01 and an enrichment of ≥1.5. The top 10 enriched terms from each GO category were selected based on ascending log P-values. Kyoto Encyclopedia of Genes and Genomes (KEGG) pathway analysis was performed using the ClueGO plugin in Cytoscape, with thresholds set to include pathways containing ≥16 genes and a κ score >0.6. A total of 11 key pathways were identified as significantly enriched.

Molecular docking analysis. Molecular docking was performed with the selected core targets. The structure of Sch B in .mol2 format was obtained from the TCMSP database (http://tcmsp-e.com/) and prepared using AutoDock Tools-1.5.6 by removing water molecules, adding hydrogen atoms and assigning atom types. Rotatable bonds were defined, and the file was saved in .pdbqt format, which can be opened and used for molecular docking with AutoDock Vina (version 1.1.2; The Scripps Research Institute).

Crystal structures of MAPK1, EGFR, ESR1, HSP90AA1, AKT1, GRB2, SRC, and HRAS in PDB format were retrieved from the PDB database (https://www.wwpdb.org/). Using PyMOL 3.7.1, non-essential small molecules were removed from the protein structures. The proteins were then processed in AutoDock Tools-1.5.6 to remove water molecules, add hydrogens and assign atom types, and these were saved as .pdbqt files.

The prepared Sch B ligand and the eight core protein receptors were subjected to molecular docking using AutoDock Vina with a batch processing script. The binding site and grid parameters were appropriately defined for each target. The resulting binding modes were visualized and analyzed using PyMOL 3.7.1.

Cell lines and culture. Human CCA HuccT1 cell line was sourced from The Cell Bank of Type Culture Collection of The Chinese Academy of Sciences. Cells were cultured in RPMI-1640 medium (Gibco; Thermo Fisher Scientific, Inc.) supplemented with 10% FBS (Gibco; Thermo Fisher Scientific, Inc.), 100 μg/ml streptomycin and 100 U/ml penicillin (HyClone™; Cytiva) and maintained in a CO_2 incubator at 37˚C. Upon reaching 80-90% confluency as observed under a microscope, cells were digested with 1 ml of trypsin containing 0.25% EDTA at 37˚C for 1-3 min. Digestion was monitored microscopically and terminated immediately when cells became rounded and detached from the culture surface.

Drugs and antibodies. Sch B was purchased from Merck KGaA and dissolved in DMSO (Merk KGaA) to create a 100 mmol/l stock solution. This stock solution was further diluted with culture media to obtain the desired concentrations. The control groups received treatment with equivalent volumes of DMSO. N-acetyl-L-cysteine (NAC) was acquired from BD Biosciences, 2',7'-dichlorofluorescein diacetate (DCFH-DA) was purchased from Merck KGaA and Bay 11-7082 was purchased from Merck KGaA. Detailed information for all primary and secondary antibodies used in this study, including antibody names, catalog numbers, dilutions and suppliers, is provided in Table I.

Reverse transcription-quantitative PCR (RT-qPCR). Total RNA was extracted from treated HuccT1 cells using TRIzol® reagent (Invitrogen; Thermo Fisher Scientific, Inc.). Subsequently, 1 μg of RNA from each sample was used for complementary DNA synthesis using the PrimeScript™ RT reagent Kit with gDNA Eraser (Takara Bio, Inc.), according to the manufacturer's protocol. For RT-qPCR, TB Green® Premix Ex Taq™ (Takara Bio, Inc.) was used on a CFX Connect Real-Time PCR Detection System (Bio-Rad Laboratories, Inc.). The thermocycling conditions were as follows: Initial denaturation at 95˚C for 30 sec, followed by 45 cycles of denaturation at 95˚C for 5 sec and combined annealing/extension at 58˚C for 30 sec. All reactions were performed in triplicate. The relative expression levels of target genes were normalized to GAPDH and calculated using the $2^{-\Delta\Delta Cq}$ method (23). The primer sequences are listed in Table II.

Table I. Details of antibodies.

Antibody name	Cat. no.	Dilution	Supplier
Primary antibodies			
BIP	3183	1:1,000	Cell Signaling Technology, Inc.
CHOP	2895	1:1,000	Cell Signaling Technology, Inc.
XBP1s	12782	1:1,000	Cell Signaling Technology, Inc.
Bax	5023	1:1,000	Cell Signaling Technology, Inc.
p-p38 MAPK (Thr180/Tyr182)	4511	1:1,000	Cell Signaling Technology, Inc.
p38 MAPK	8690	1:1,000	Cell Signaling Technology, Inc.
p-p65 NF-κB (Ser536)	3033	1:1,000	Cell Signaling Technology, Inc.
p65 NF-κB	8242	1:1,000	Cell Signaling Technology, Inc.
p-IκBα (Ser32)	2859	1:1,000	Cell Signaling Technology, Inc.
IκBα	4814	1:1,000	Cell Signaling Technology, Inc.
IL-6	12153	1:1,000	Cell Signaling Technology, Inc.
IL-8	94407	1:1,000	Cell Signaling Technology, Inc.
TNF-α	6945	1:1,000	Cell Signaling Technology, Inc.
GAPDH	5174	1:5,000	Cell Signaling Technology, Inc.
Secondary antibodies			
Anti-rabbit IgG, HRP-linked	7074	1:3,000	Cell Signaling Technology, Inc.
Anti-mouse IgG, HRP-linked	7076	1:3,000	Cell Signaling Technology, Inc.
AP-labeled Anti-rabbit IgG	WB0120	1:5,00	Vigorous Biotechnology Beijing Co., Ltd.

P, phosphorylated; HRP, horse radish peroxidase.

Table II. Primer sequences.

Target gene	Primer sequence (5' to 3')
GAPDH-FP	GAAGGTGAAGGTCGGAGTC
GAPDH-RP	GAAGATGGTGATGGGATTTC
XBP1s-FP	AGGAGTTAAGACAGCGCTTGGGG
XBP1s-RP	AATACCTGCACCTGCTGCGGACTC AGCAGA
BIP-FP	TGACATTGAAGACTTCAAAGCT
BIP-RP	CTGCTGTATCCTCTTCACCAGT
CHOP-FP	CAACTGCAGAGATGGCAGCTGA
CHOP-RP	CTGATGCTCCCAATT GTTCAT
IL6-FP	TCAGGGATGCAATGCCACTT
IL6-RP	TGCAGAAGAGAGCCAACCAA
IL8-FP	ACAAGCTTCTAGGACAAGAGCC
IL8-RP	ACTTCTCCACAACCCTCTGC
TNFα-FP	CGAGTGACAAGCCTGTAGC
TNFα-RP	CCTTCTCCAGCTGGAAGAC

FP, forward primer; RP, reverse primer.

Western blot analysis. HuccT1 cells were treated with various concentrations of Sch B (0, 40, 80 and 160 μM) for 48 h at 37˚C. After treatment, cells were harvested and lysed on ice using RIPA buffer (Beyotime Biotechnology) supplemented with a protease inhibitor cocktail (Roche Applied Science) for 15 min. The lysates were centrifuged at 13,500 x g for 30 min at 4˚C to collect the supernatant. Protein concentration was determined using the BCA assay. Subsequently, 60 μg of total protein per sample was separated by SDS-PAGE on 10% polyacrylamide gels and electrophoretically transferred onto PVDF membranes (MilliporeSigma). Following transfer, the membranes were blocked with 5% skim milk prepared in Tris-buffered saline with Tween-20 (TBST) for 2 h at room temperature. The membranes were then incubated overnight at 4˚C with the indicated primary antibodies (Table I). After incubation, the membranes were washed three times for 10 min each with TBST. A total of two distinct detection systems were employed: Horseradish Peroxidase (HRP)-chemiluminescence detection: For HRP-based detection, the membranes were incubated with appropriate HRP-conjugated secondary antibodies for 1 h at room temperature. After washing with TBST, protein bands were visualized using an enhanced chemiluminescence substrate and imaged with a Gel Doc 2000 system (Bio-Rad Laboratories, Inc.). Alkaline Phosphatase (AP)-colorimetric detection: For AP-based colorimetric detection, an AP western detection kit (Vigorous Biotechnology Beijing Co., Ltd.) was used. After primary antibody incubation and washing, the membranes were probed with AP-conjugated secondary antibodies for 30 to 120 min at room temperature. The membranes were then thoroughly washed 3-5 times with TBST to remove any phosphate residues. A color development solution was freshly prepared immediately before use by adding 0.1 ml of 5-bromo-4-chloro-3-indolyl phosphate (BCIP) and 0.1 ml of nitroblue tetrazolium (NBT) per 10 ml of reaction buffer (Vigorous Biotechnology, Beijing Co., Ltd.). After removing the wash buffer, sufficient development solution was added to completely cover the membrane, followed by incubation at

room temperature for 5 to 15 min in the dark, with close monitoring of band intensity. The reaction was stopped by rinsing the membrane with distilled water once the target bands were clearly visible with minimal background. The membrane was air-dried and imaged directly.

Measurement of ROS production. HuccT1 cells were prepared as single cell suspensions and then seeded in 6-well plates at a density of $1x10^6$ cells per well in 100 μl of culture medium. Subsequently, the cells were treated with various concentrations of Sch B (0, 40 and 160 μM) for 24 h at 37˚C in a CO_2 incubator. DCFH-DA was diluted with serum-free medium at a ratio of 1:1,000 to reach a final concentration of 10 μmol/l. The CCA cells were incubated with DCFH-DA at 37˚C for 20 min. Following three washes with PBS, the cells were stimulated using a positive control for ROS. Finally, the excitation and emission wavelengths for the fluorescence enzyme were adjusted to 488 and 525 nm, respectively.

Lactate dehydrogenase (LDH) release assay. An LDH release assay was performed according to the manufacturer's protocol (Beyotime Biotechnology). The amount of color formed is proportional to the number of lysed cells. Cells treated with DMSO or 160 μmol/l Sch B + different concentrations of NAC (0, 0.5, 1, 3, 6 μmol/l) were seeded in a 96-well plate. After 24 h, LDH levels were determined by analyzing the amount of LDH released into the cell culture supernatant. Absorbance signals at 490 nm were obtained using a microplate reader. To determine the percentage of LDH release, the experimental LDH release quantities were calculated relative to the control LDH release quantities, as stated in the provided instructions.

Cell viability assay by calcein AM-PI. HuccT1 cells were treated with Sch B (0 and 160 μM) in the presence or absence of various concentrations of NAC (0, 0.5, 1, 3 and 6 μM) for 24 h at 37°C. After treatment, cells were incubated with 2 μM calcein-AM (CAS 148504-34-1; MedChemExpress) for 20 min at 37˚C, followed by a 5 min co-incubation with 4 μM propidium iodide (PI; CAS 25535-16-4; MedChemExpress) at 37˚C. Fluorescence images were captured using a Cytation 3 Cell Imaging Multi-Mode Reader (Agilent Technologies, Inc.) with excitation at 488 nm and emission recorded at 525 nm for calcein-AM.

Dual luciferase reporter gene experiment. HuccT1 cells were seeded in 24-well plates and cultured for 24 h at 37˚C in a 5% CO_2 atmosphere prior to transfection. Cells were co-transfected with 100 ng of reporter plasmid (pGL4.2-3xAP-1-Luc or pGL4.2-NF-κB-Luc, both from Promega Corporation) and 1 ng of internal control plasmid (pRL-TK, Promega Corporation), corresponding to a mass ratio of 100:1 (reporter:internal control), using Lipofectamine® 2000 (Invitrogen; Thermo Fisher Scientific, Inc.). Transfection was performed at 37˚C, and the medium was replaced with fresh culture medium 4 h post-transfection. At 24 h post-transfection, cells were treated with various concentrations of Sch B (0, 10, 20, 40, 80 and 160 μM) for an additional 24 h at 37˚C. After treatment, the culture medium was removed, and cells were lysed with Reporter Gene Cell Lysis Buffer (Beyotime Biotechnology). A 20 μl aliquot of cell lysate was used to measure firefly and Renilla luciferase activities sequentially using the Dual Luciferase Reporter Gene Assay Kit II (cat. no. RG029; Beyotime Biotechnology) on a luminometer. Relative luciferase activity was calculated as the ratio of firefly luminescence to Renilla luminescence.

Colony formation assay. After cell counting, the HuccT1 cells were diluted to $1x10^5$ cells/ml, then $1x10^4$ cells/ml was inoculated on a 6-well plate (100 μl/well). After inoculation, complete medium was added (2 ml/well). After 1 week of culture at 37˚C in 5% CO_2, the medium was removed and cells were rinsed twice with PBS or normal saline for 10 sec each, fixed with 4% paraformaldehyde for 15 min at room temperature, and washed twice with PBS twice for 10 sec each. Subsequently, 200 μl of crystal violet staining solution was added to cover the bottom of each well and incubation for 20 min at room temperature. The 6-well plate was then rinsed under running water for 10 sec, air-dried, and the number of colonies (containing >50 cells) was counted manually.

Immunofluorescent staining. HuccT1 cells were cultured on circular coverslips in 6-well plates, fixed with 4% paraformaldehyde for 30 min at room temperature, and then permeabilized with 0.3% Triton X-100 (Merck KGaA) for 15 min at room temperature. Following permeabilization, cells were incubated in a solution containing 5% bovine serum albumin (Merck KGaA) for 40-60 min at room temperature. After washing three times with PBS, the cells were incubated overnight at 4˚C with the corresponding primary antibodies (dilution 1:100; Table I). The next day, cells were washed three times with PBS and incubated with fluorescence-labeled secondary antibodies (dilution 1:200; Table I) for 1 h at room temperature in the dark. Subsequently, cells were stained with Hoechst 33342 (cat. no. HY-D0983; MedChemExpress) for 15 min at room temperature in the dark. The coverslips were then mounted onto glass slides, and fluorescence images were captured using a Nikon fluorescence microscope (Nikon Corporation).

Statistical analysis. The data are presented as mean ± SD from at least three independent experiments. Statistical analyses were performed using SPSS 23.0 (IBM Corp.). All datasets were confirmed to follow a normal distribution by the Shapiro-Wilk test. For comparisons among multiple experimental groups with a single control group, homogeneity of variances was assessed using Brown-Forsythe test. When the assumption of homogeneity of variances was met, ANOVA followed by Dunnett's post hoc test was applied to compare each experimental group with the control group. In cases where variances were heterogeneous, Welch's ANOVA followed by Dunnett T3 post hoc test was employed. The specific statistical test used for each dataset is indicated in the corresponding figure legend. A value of $^{*}P<0.05$, $^{**}P<0.01$ and $^{***}P<0.001$ was considered to indicate a statistically significant difference.

Results

Identification of core targets and validation by molecular docking. Potential targets of Sch B and CCA were retrieved from relevant databases. A Venn diagram revealed 120 overlapping targets between Sch B and CCA (Fig. 1A). A PPI network was

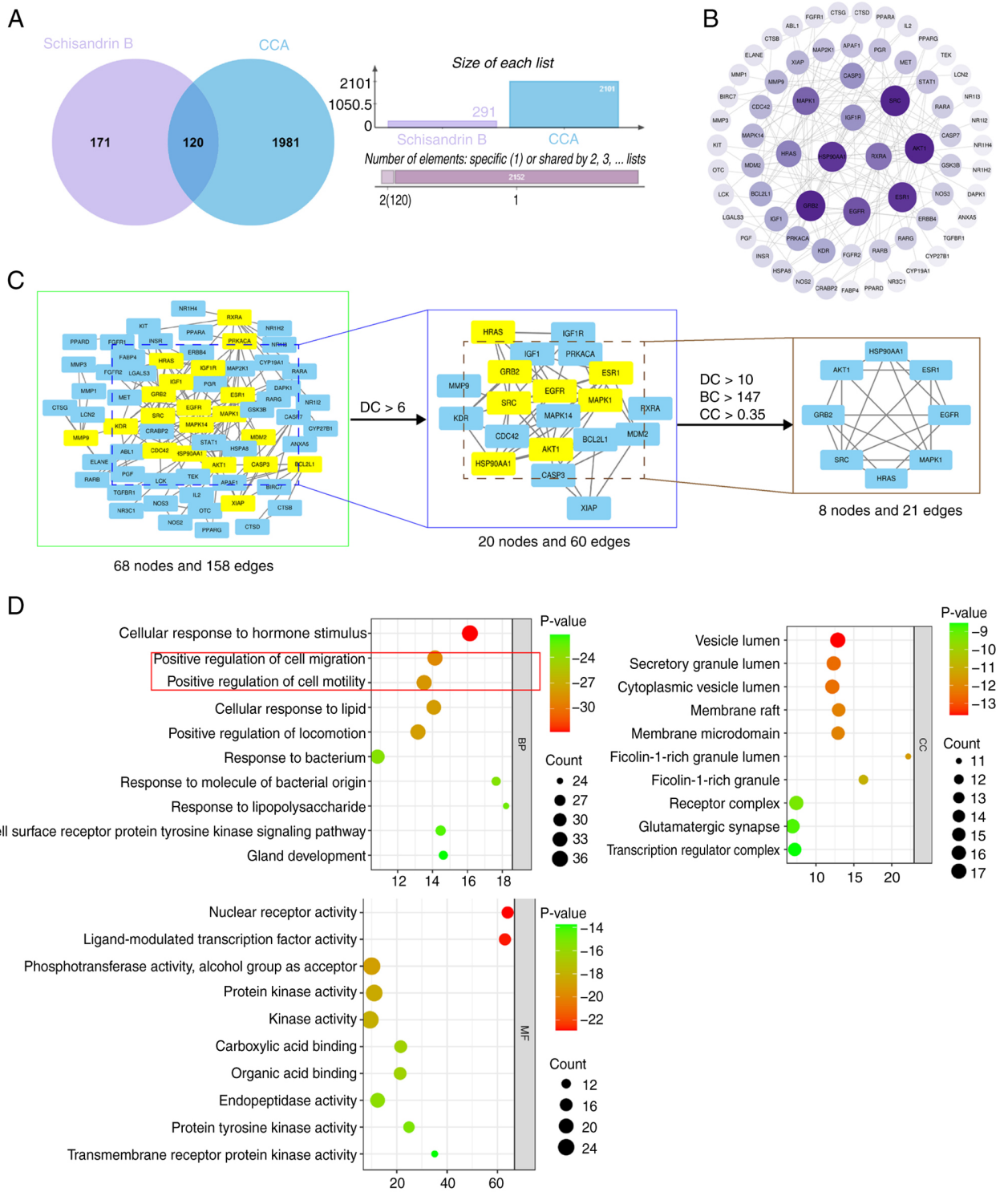

Figure 1. Identification of core targets and functional enrichment via network pharmacology. (A) Venn diagram showing the overlapping targets between Schisandrin B and CCA. (B) Protein-protein interaction network of the common targets between Sch B and CCA. Node size is proportional to the Degree value in the network. (C) Screening process of the PI network topology. A total of eight core targets were identified from 120 common targets based on DC, BC and CC. (D) Gene Ontology enrichment analysis bubble chart displaying the top 10 enriched terms in biological process, cellular component and molecular function. The y-axis and x-axis represent the term description and gene ratio, respectively. Bubble color and size reflect the-$\log_{10}$ (P-value) and the number of genes involved, respectively. CCA, cholangiocarcinoma; DC, degree centrality; BC, betweenness centrality; CC, closeness centrality.

constructed, comprising 68 nodes and 158 edges, with node size proportional to the degree value (Fig. 1B). Using a DC threshold >6, a subnetwork with 20 nodes and 60 edges was obtained. Further applying criteria of DC >10, BC >147 and CC >0.35, a core network of 8 nodes and 21 edges was identified. A total of eight core targets were ultimately selected: MAPK1, EGFR, ESR1, HSP90AA1, AKT1, GRB2, SRC and HRAS (Fig. 1C).

GO enrichment analysis of the 120 overlapping targets was performed, covering BP, cellular component and MF categories. The top 10 enriched terms from each category are

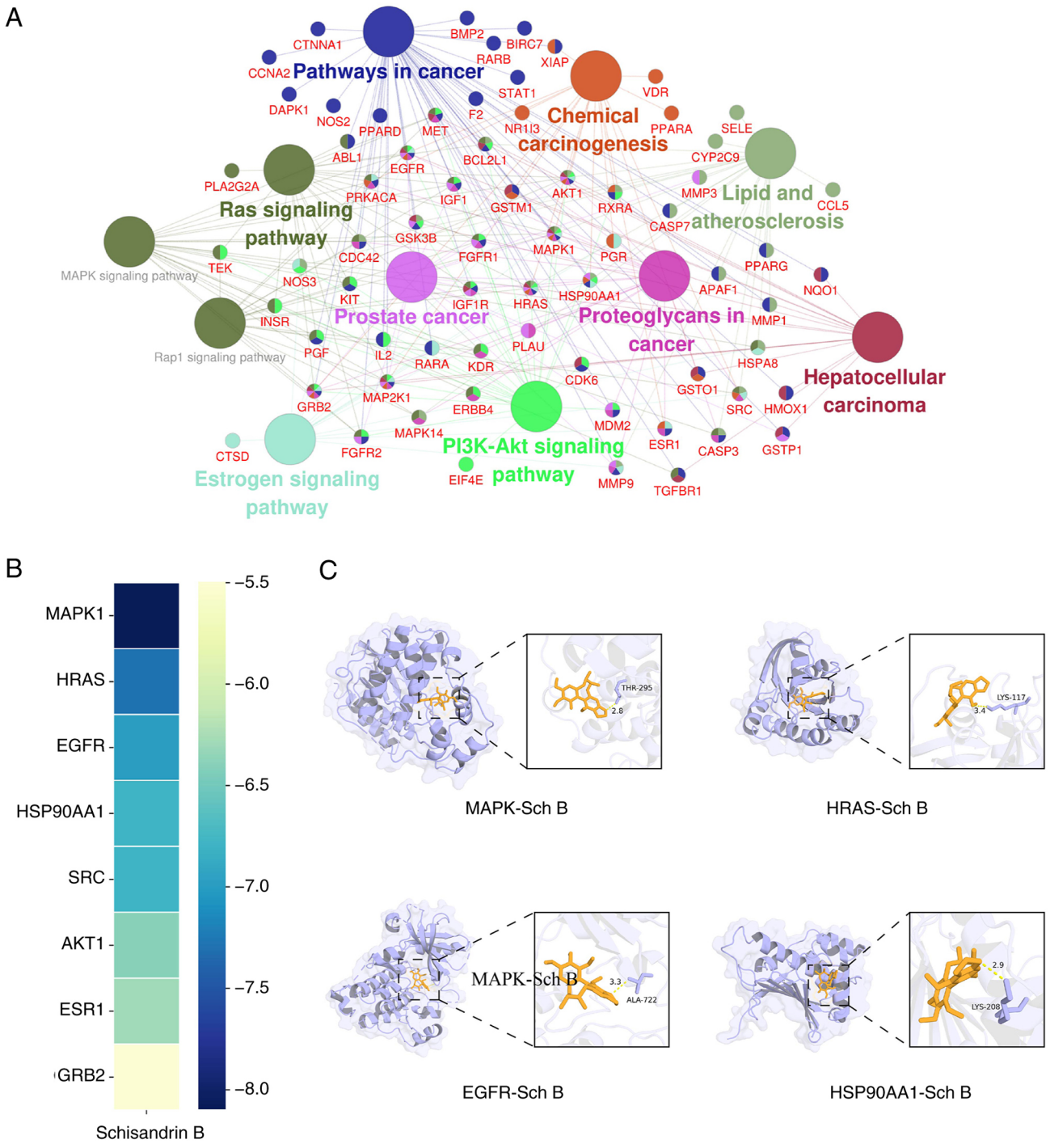

Figure 2. KEGG enrichment analysis and molecular docking validation of core targets. (A) Visualization of KEGG pathway enrichment analysis for the core targets. (B) Heatmap depicting the molecular docking binding energies between Sch B and the eight candidate core targets. (C) Representative molecular docking poses illustrating the binding modes of Sch B with four key targets. KEGG, Kyoto Encyclopedia of Genes and Genomes; Sch B, Schisandrin B.

displayed in a bubble chart (Fig. 1D), suggesting that Sch B may regulate the migration and motility of CCA cells.

KEGG pathway analysis was conducted using the ClueGO plugin in Cytoscape 3.8.0, with thresholds set to include pathways containing ≥16 genes and a κ score >0.6. A total of 11 significantly enriched pathways were identified, primarily associated with 'Pathways in cancer' and the 'MAPK signaling pathway' (Fig. 2A). Molecular docking was performed between Sch B and the top 8 core target proteins (MAPK1, EGFR, ESR1, HSP90AA1, AKT1, GRB2, SRC and HRAS) identified from the PPI network. The lowest binding energies for all ligand-receptor complexes were below-5 kcal/mol, indicating spontaneous binding and stable conformations (Table III). Among them, MAPK1 exhibited the strongest binding affinity with Sch B. The binding modes of Sch B with MAPK1, HRAS, EGFR and HSP90AA1 were visualized using PyMOL 3.7.1 (Fig. 2B and C).

Sch B induced a dose-dependent increase in ROS levels in CCA cells. Based on the KEGG pathway enrichment analysis, which indicated strong associations between the predicted

Table III. Molecular docking binding affinity of Sch B with core targets.

Compound	Lowest binding energy (kcal/mol)
MAPK1	-8.1
EGFR	-7
HRAS	-7.3
HSP90AA1	-6.8
AKT1	-6.4
GRB2	-5.5
SRC	-6.8
ESR1	-6.3

MAPK signaling pathway and key BPs such as chemical carcinogenesis, and supported by established literature evidence highlighting the pivotal role of oxidative stress as a key mediator in these pathways, the present study was guided to investigate the involvement of ROS in the mechanism of Sch B. Guided by these predictions, the biological effects were subsequently validated through a series of *in vitro* experiments. CCA cells were exposed to various concentrations of Sch B, ranging from 0 to 160 μmol/l, to assess the mRNA expression levels of BIP, CHOP and XBP1s. The results showed an increasing trend, indicative of a dose-dependent effect (Fig. 3A-C). Western blot analysis further confirmed the elevated expression levels of BIP, CHOP and XBP1s, showing an upward trend (Fig. 3D).

To support these findings, a ROS probe, DCFH-DA and flow cytometry were used to measure ROS levels in CCA cells. The results demonstrated a dose-dependent increase in ROS levels (Fig. 3E and F). Collectively, these results suggest that Sch B induces a dose-dependent increase in ROS levels within CCA cells, offering valuable insights into its molecular impact on cellular responses.

NAC counteracted the upregulatory effect of Sch B on ROS expression. Treatment with 160 μmol/l Sch B led to a notable increase in the expression levels of BIP, CHOP and XBP1s in CCA cells. The addition of NAC showed a dose-dependent reduction in the expression levels of BIP, CHOP and XBP1s in the experimental group (Fig. 4A and B).

It is well known that NAC, as an antioxidant, can reduce ROS levels and protect cell membrane integrity (24,25), thereby lowering LDH release from cells. With increasing concentrations of NAC, the activity of LDH in the culture medium decreases (Fig. 4C), A reduction in Bax expression was observed only at the highest concentration of NAC (6 μM). Western blotting results in Fig. 4E are representative images and were not subjected to densitometric quantification. In parallel, Calcein-AM/PI staining showed that Sch B-induced cytotoxicity was alleviated by NAC co-treatment, as evidenced by increased green fluorescence intensity (Fig. 4D). Consequently, these results show that NAC may counter the inhibitory effects of Sch B on CCA cells proliferation and facilitate apoptosis by mitigating ROS upregulation.

MAPK signaling pathway inhibition by Sch B. CCA cells treated with different concentrations of Sch B ranging from 0 to 160 μmol/l showed a dose-dependent decrease in AP-1 expression, a key regulatory component of the MAPK signaling pathway, as measured by a double luciferase reporter assay (Fig. 5A). Additionally, western blot analysis indicated a decreasing trend in p-p38 expression with higher Sch B concentrations, further demonstrating inhibition of the MAPK signaling pathway (Fig. 5C).

Treatment with 160 μmol/l Sch B led to significant inhibition of CCA cell activity (Fig. 5B). The subsequent addition of SB203580, a p38 MAPK inhibitor, at 0.2 and 0.5 μmol/l concentrations resulted in a notable decrease in CCA cell activity compared with the control group (Fig. 5B), reflecting the effects seen with Sch B.

Furthermore, the anti-proliferative effect of Sch B on CCA cells was evidenced by a trend of reduced colony formation at 160 μM, an effect qualitatively similar to that observed with 0.5 μM SB203580 (representative images shown in Fig. 5D). These findings together highlight the effectiveness of Sch B in impeding the MAPK signaling pathway and reducing CCA cell proliferation.

Sch B inhibits NF-κB signaling pathway expression. Sch B exhibited dose-dependent suppression of the NF-κB signaling pathway in CCA cell lines. Treatment with Sch B (0,40, 80, 160 μmol/l) led to a corresponding decrease in the expression levels of IL-6, IL-8 and TNF-α. Although the 40 μmol/l treatment group generally did not show statistically significant differences compared to the control group, a trend of reduction was observed with increasing concentrations (Fig. 6A-C). The suppressive effect on NF-κB expression was shown by a dose-dependent reduction in NF-κB levels, as shown by a double luciferase assay (Fig. 6D).

In the experimental group, 160 μmol/l Sch B notably reduced CCA cell activity. To directly and visually assess the effect of Sch B on p65 translocation, the present study performed immunofluorescence staining for p65. The results demonstrate nuclear accumulation of p65 in control cells (without Sch B treatment), whereas in Sch B-treated cells, p65 was predominantly retained in the cytoplasm, with correspondingly lower nuclear levels (Fig. 6E). Bay 11-7082 is a selective NF-κB inhibitor that suppresses IκBα phosphorylation (26), thereby preventing IκBα degradation and NF-κB nuclear translocation, which ultimately inhibits downstream NF-κB-dependent gene transcription. Accordingly, CCA cell activity was significantly reduced following the addition of Bay 11-7082 in a dose-dependent manner, with both 2 and 5 μM concentrations showing significant decreases compared with the control group (Fig. 6F). These results highlight the effectiveness of Sch B in inhibiting the NF-κB signaling pathway, resulting in the suppression of CCA cell activity.

Discussion

According to reports, over the past few decades, the incidence of CCA, a rare but highly malignant disease, has rapidly increased (1,2). It has become the second most common primary liver cancer in humans, following hepatocellular carcinoma, and is emerging as a major global health issue (3).

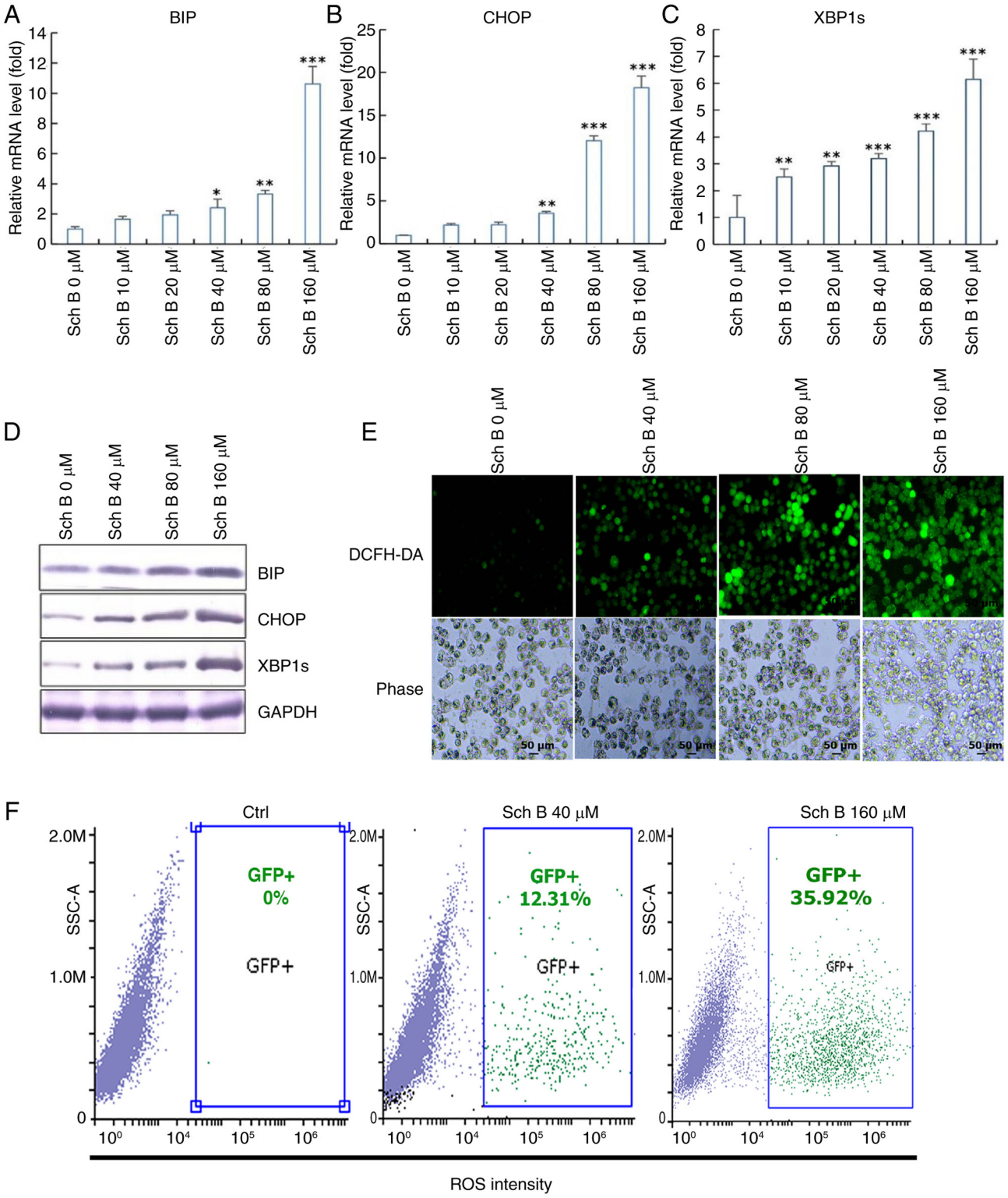

Figure 3. Sch B induced a dose-dependent increase in ROS levels in CCA cells. (A) BIP, (B) CHOP and (C) XBP1s expressions were determined by reverse-transcription quantitative PCR in CCA cells treated with different concentrations of Sch B (0, 10, 20, 40, 80, 160 μmol/l), (D) BIP, CHOP and XBP1s expression levels were determined by western blotting in CCA cells treated with different concentrations of Sch B (0, 40, 80, 160 μmol/l). (E) ROS levels in CCA cells treated with different concentrations of Sch B (0, 40, 80, 160 μmol/l) were measured using the ROS probe DCFH-DA. (F) Flow cytometry analysis of ROS levels in CCA cells following treatment with various Sch B concentrations (0, 40, 160 μmol/l). Statistical analysis was performed using ANOVA and Dunnett's post hoc test. *P<0.05, **P<0.01, ***P<0.001. CCA, cholangiocarcinoma; Sch B, Schisandrin B; Ctrl, control; ROS, reactive oxygen species.

Currently, surgical resection remains the primary treatment for CCA. However, due to the insidious onset of the disease and tendency to metastasize, only 20-40% of patients with potentially resectable disease undergo surgery. Consequently, the majority of patients require systemic treatment, including systemic chemotherapy with drugs such as gemcitabine, cisplatin, 5-fluorouracil and capecitabine (27). However, the development of drug resistance to chemotherapy poses an

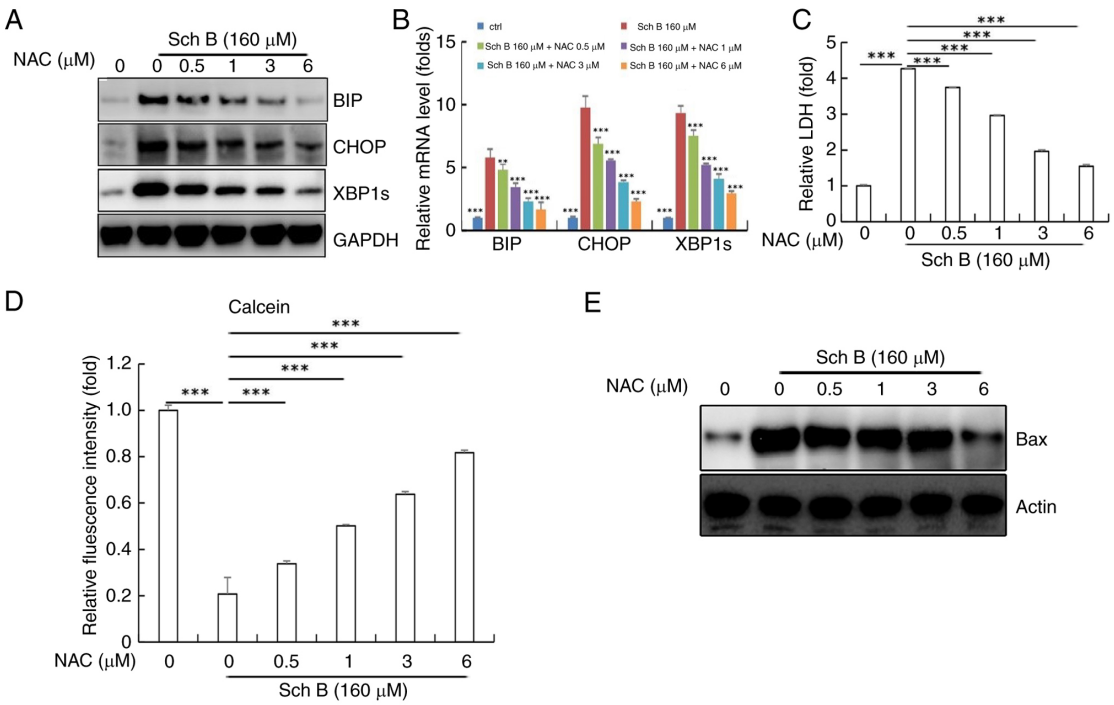

Figure 4. NAC counteracted the upregulatory effect of Sch B on ROS expression. After treatment with 160 μmol/l Sch B + different concentrations of NAC (0, 0.5, 1, 3, 6 μmol/l). BIP, CHOP and XBP1s expression determined by (A) western blotting and (B) reverse transcription-quantitative PCR in CCA cells. (C) LDH activity in cell culture medium. (D) Cell activity levels detected by the Calcein AM-PI live cell staining. (E) Western blot analysis of the expression levels of Bax in CCA cells. Statistical analysis was performed using ANOVA and Dunnett's post hoc test. **P<0.01, ***P<0.001. ROS, reactive oxygen species; CCA, cholangiocarcinoma; NAC, N-acetyl-L-cysteine; ctrl, control; Sch B, Schisandrin B; LDH, lactate dehydrogenase.

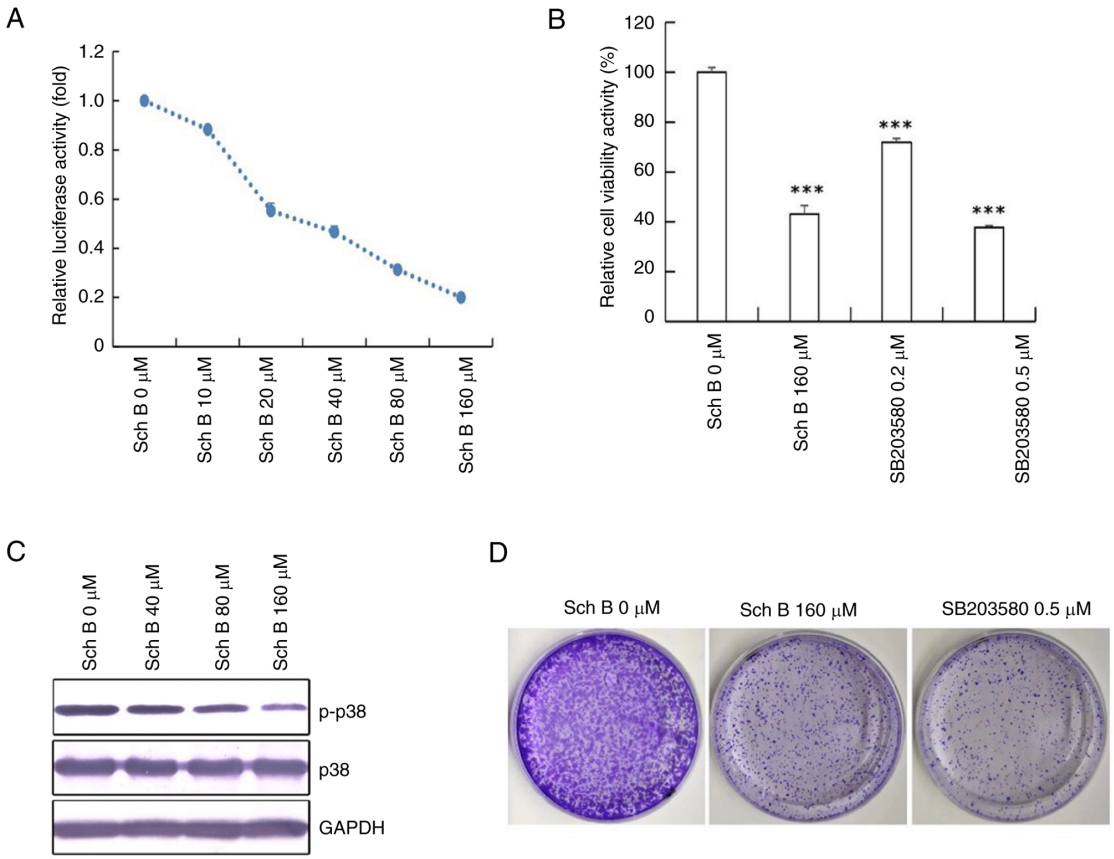

Figure 5. MAPK signaling pathway inhibition by Sch B. (A) A double luciferase assay analysis of the expression of AP-1 in CCA cells treated with different concentrations of Sch B (from 0 to 160 μmol/l). (B) To evaluate the activity of CCA cells, they were separately treated with Sch B and the MAPK-specific inhibitor SB203580. (C) Western blot analysis of the expression levels of p-p38 and p38. (D) Colony formation assay of CCA cells treated with 160 μmol/l Sch B and 0.5 μmol/l SB203580. Statistical analysis was performed using ANOVA and Dunnett's post hoc test. ***P<0.001. Sch B, Schisandrin B; P, phosphorylated.

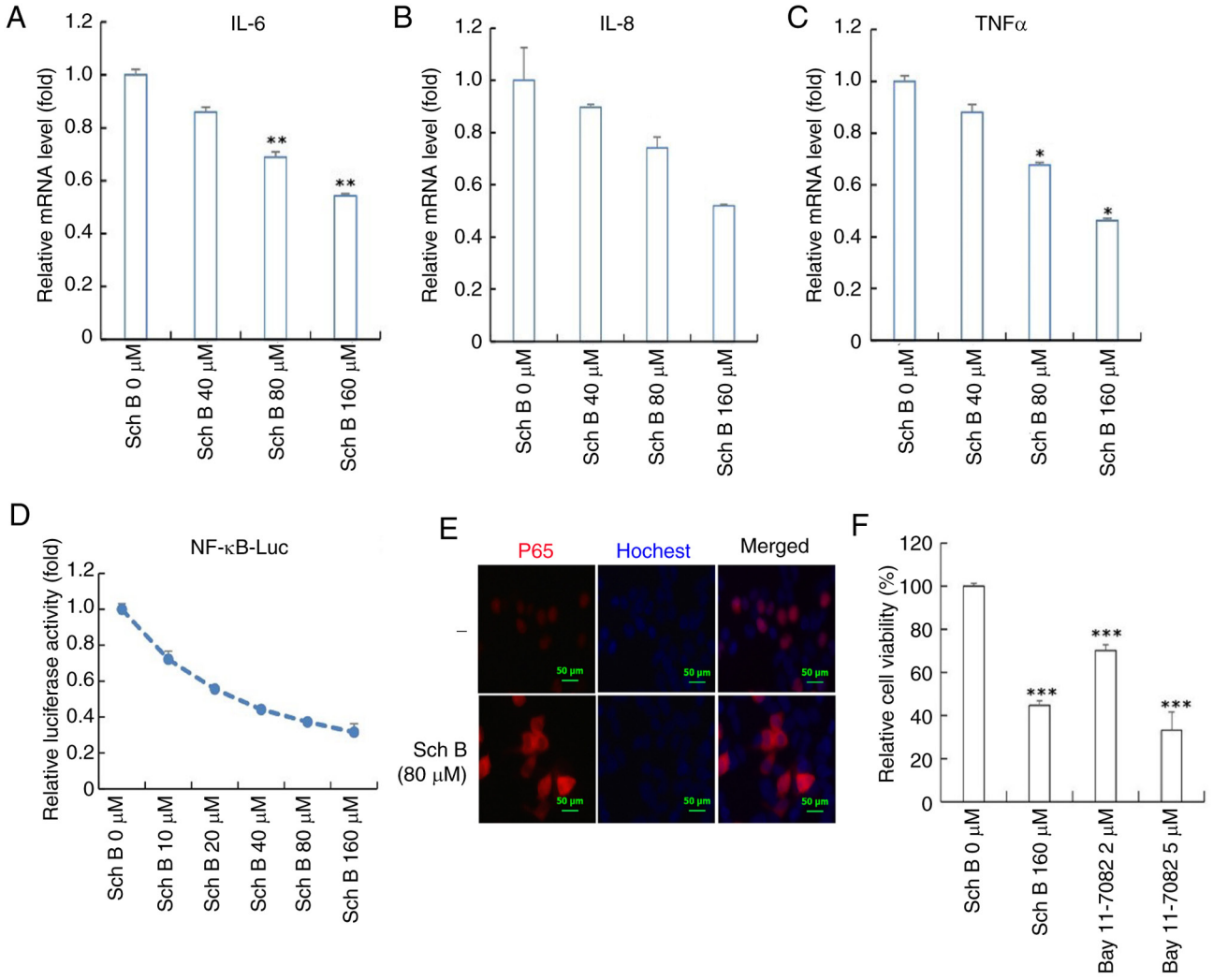

Figure 6. Sch B inhibits NF-κB signaling pathway expression. mRNA expression levels of (A) IL-6, (B) IL-8 (C) and TNF-α were measured in CCA cells treated with different concentrations of Sch B (0, 40, 80, 160 μmol/l). Statistical analysis was performed using Welch's ANOVA followed by Dunnett's T3 post hoc test. (D) NF-κB expression in CCA cells was evaluated using a double luciferase assay with different concentrations of Sch B (0, 10, 20, 40, 80, 160 μmol/l). (E) Hoechst immunofluorescence staining of p65 expression in CCA cells. (F) CCA cell activity was assessed after treatment with Sch B and Bay 11-7082, a targeted NF-κB inhibitor. Statistical analysis was performed using ANOVA and Dunnett's post hoc test. *P<0.05, **P<0.01, ***P<0.001. Sch B, Schisandrin B; CCA, cholangiocarcinoma.

additional challenge to the treatment of CCA. Therefore, it is important to find new and safe drugs for treating CCA.

Currently, an increasing number of researchers are focusing on traditional Chinese medicine extracts, which are considered to contain various active ingredients capable of acting on multiple molecular targets and signaling pathways simultaneously (28-30). These extracts have relatively low side effects and are suitable for long-term use. Among these compounds, Sch B has been demonstrated to exert therapeutic effects in various malignant tumors (7-10). One report indicates that Sch B may inhibit the viability and proliferation of gallbladder cancer cells and promote apoptosis, highlighting its potential as a therapeutic agent for gallbladder cancer (8).

The present study first employed network pharmacology to predict the potential targets of Sch B in CCA. Functional enrichment analysis revealed significant enrichment of these targets in cancer-related pathways and the MAPK signaling pathway. Molecular docking further confirmed the strong binding affinity between Sch B and core targets, including MAPK.

The present *in vitro* study demonstrated that Sch B exerts its anti-CCA effects, at least in part, by modulating ROS levels. ROS play a dual role in tumorigenesis, acting as signaling molecules at low to moderate concentrations to promote tumor survival via pathways such as MAPK/ERK1/2, p38MAPK, JNK and PI3K/Akt, leading to activation of downstream effectors including NF-κB, MMP and vascular endothelial growth factor. By contrast, high concentrations of ROS trigger apoptotic pathways (31-33). Results of the present study revealed that Sch B treatment dose-dependently upregulated the expression of endoplasmic reticulum stress-related molecules (BIP, CHOP and XBP1s) and significantly increased ROS levels in CCA cells, while also inhibiting proliferation and promoting the expression of the pro-apoptotic protein Bax. The ROS scavenger NAC reversed these effects, restoring cell viability and reducing apoptosis, confirming that Sch B primarily exerts its anti-CCA activity through ROS elevation.

Studies have established that ROS influence multiple signaling pathways, notably the MAPKs and NF-κB transduction cascades (34,35). ROS play a key role in activating

the MAPK signaling pathway (34) and are involved in p38 activation (35). Upon activation by oxidative stress, the MAPK signaling pathway compromises cellular anti-apoptotic capacity, leading to caspase activation and apoptosis induction. Additionally, p38MAPK has been shown to modulate the transcriptional activity of NF-κB, enabling NF-κB p65 nuclear translocation and subsequent activation of downstream signaling pathways (36,37). The NF-κB signaling pathway promotes CCA cell proliferation, metastasis and invasion (38).

In the present study, increasing concentrations of Sch B led to decreased p-p38 expression and reduced AP-1 activity, accompanied by inhibited cell proliferation. Concurrently, expression of p-p65 and p-IκBα increased, while downstream inflammatory factors IL-6, IL-8 and TNF-α decreased. Immunofluorescence staining revealed reduced nuclear translocation of p65, indicating suppression of the NF-κB pathway. The use of the p38MAPK inhibitor SB203580 and the NF-κB inhibitor Bay 11-7082 further suppressed CCA cell viability, suggesting a role for these pathways in the mechanism of Sch B.

The *in vitro* findings of the present study provide valuable mechanistic insights, however, several important limitations must be acknowledged. Firstly, the inherent constraints of cell-based models cannot fully replicate the complex *in vivo* tumor microenvironment, including key factors such as cell-cell interactions, tissue architecture and pharmacokinetic processes such as drug metabolism, distribution and clearance, all of which may substantially influence therapeutic outcomes. Secondly, and more specifically to the present study, the mechanistic conclusions are derived primarily from experiments using a single human CCA cell line (HuccT1). This approach does not capture the known heterogeneity of CCA among patients and the absence of a parallel normal cholangiocyte control line precludes a definitive assessment of the selective toxicity of Sch B against cancer cells. Consequently, the generalizability of the present findings is currently limited. To address these points, future work will extend these investigations to other representative CCA cell lines (for example, RBE and TFK-1) and include normal human intrahepatic biliary epithelial cells (for example, HIBEC) for a thorough evaluation of broader applicability and selectivity. Ultimately, *in vivo* validation using appropriate animal models will be essential to confirm the anti-tumor efficacy and biosafety of Sch B and to pave the way for its potential clinical translation.

In conclusion, the present findings demonstrate that Sch B may suppress proliferation and induces apoptosis in CCA cells by elevating intracellular ROS levels, mechanistically associated with the modulation of the p38MAPK/NF-κB signaling pathway. As a natural compound, Sch B exhibits multi-target intervention characteristics, underscoring its potential for clinical translation. Future studies will focus on *in vivo* validation of its antitumor efficacy and biosafety, and explore combination strategies with conventional cytotoxic agents to elucidate synergistic mechanisms. These efforts will provide a stronger experimental foundation for developing Sch B as a promising therapeutic candidate against CCA.

Acknowledgements

Not applicable.

Funding

No funding was received.

Availability of data and materials

All data generated in the present study may be requested from the corresponding author.

Authors' contributions

JY and SW confirmed the authenticity of all raw data. The conception and design of the study were carried out by JY, SW, WL and XW. Data acquisition was performed by JY, WL and XY. Data analysis and interpretation were conducted by WL, XY and QH. Manuscript writing and/or revision were undertaken by JY and WL. Administrative, technical or material support was provided by SW and XY. Study supervision was managed by SW. All authors read and approved the final version of the manuscript.

Ethics approval and consent to participate

Not applicable.

Patient consent for publication

Not applicable.

Competing interests

The authors declare that they have no competing interests.

References

1. Li X, Guan R and Zhang S: Factors contributing to the high malignancy level of cholangiocarcinoma and its epidemiology: Literature review and data. Biology (Basel) 14: 351, 2025.
2. Ilyas SI, Khan SA, Hallemeier CL, Kelley RK and Gores GJ: Cholangiocarcinoma-evolving concepts and therapeutic strategies. Nat Rev Clin Oncol 15: 95-111, 2018.
3. Bridgewater J, Galle PR, Khan SA, Llovet JM, Park JW, Patel T, Pawlik TM and Gores GJ: Guidelines for the diagnosis and management of intrahepatic cholangiocarcinoma. J Hepatol 60: 1268-1289, 2014.
4. Peery AF, Crockett SD, Murphy CC, Lund JL, Dellon ES, Williams JL, Jensen ET, Shaheen NJ, Barritt AS, Lieber SR, *et al*: Burden and cost of gastrointestinal, liver, and pancreatic diseases in the united states: Update 2018. Gastroenterology 156: 254-272. e11, 2019.
5. Razumilava N and Gores GJ: Cholangiocarcinoma. Lancet 383: 2168-2179, 2014.
6. Qi L, Yu HQ, Li YQ, Jin H, Zhao DH and Xu Y: Schidandrin B kills tumor cells by initiating apoptosis in glioma SHG-44 cells. Chin J Integr Med: Aug 2, 2016 doi: 10.1007/s11655-015-2406-9 (Epub ahead of print).
7. Li Q, Lu XH, Wang CD, Cai L, Lu JL, Wu JS, Zhuge QC, Zheng WM and Su ZP: Antiproliferative and apoptosis-inducing activity of schisandrin B against human glioma cells. Cancer Cell Int 15: 12, 2015.
8. Xiang SS, Wang XA, Li HF, Shu YJ, Bao RF, Zhang F, Cao Y, Ye YY, Weng H, Wu WG, *et al*: RETRACTED: Schisandrin B induces apoptosis and cell cycle arrest of gallbladder cancer cells. Molecules 19: 13235-13250, 2014.
9. Dai X, Yin C, Guo G, Zhang Y, Zhao C, Qian J, Wang O, Zhang X and Liang G: Schisandrin B exhibits potent anticancer activity in triple negative breast cancer by inhibiting STAT3. Toxicol Appl Pharmacol 358: 110-119, 2018.

10. Nasser MI, Han T, Adlat S, Tian Y and Jiang N: Inhibitory effects of Schisandrin B on human prostate cancer cells. Oncol Rep 41: 677-685, 2019.
11. Zhang H, Chen Q, Dahan A, Xue J, Wei L, Tan W and Zhang G: Transcriptomic analyses reveal the molecular mechanisms of schisandrin B alleviates CCl4-induced liver fibrosis in rats by RNA-sequencing. Chem Biol Interact 309: 108675, 2019.
12. Sabharwal SS and Schumacker PT: Mitochondrial ROS in cancer: Initiators, amplifiers or an Achilles' heel? Nat Rev Cancer 14: 709-721, 2014.
13. Trinh VH, Nguyen Huu T, Sah DK, Choi JM, Yoon HJ, Park SC, Jung YS and Lee SR: Redox regulation of PTEN by reactive oxygen species: Its role in physiological processes. Antioxidants (Basel) 13: 199, 2024.
14. Caligiuri A, Becatti M, Porro N, Borghi S, Marra F, Pastore M, Taddei N, Fiorillo C and Gentilini A: Oxidative stress and Redox-dependent pathways in cholangiocarcinoma. Antioxidants (Basel) 13: 28, 2023.
15. Srinivas US, Tan BWQ, Vellayappan BA and Jeyasekharan AD: ROS and the DNA damage response in cancer. Redox Biol 25: 101084, 2019.
16. Marchi S, Guilbaud E, Tait SWG, Yamazaki T and Galluzzi L: Mitochondrial control of inflammation. Nat Rev Immunol 23: 159-173, 2023.
17. Glover HL, Schreiner A, Dewson G and Tait SWG: Mitochondria and cell death. Nat Cell Biol 26: 1434-1446, 2024.
18. Wandee J, Srinontong P, Prawan A, Senggunprai L, Kongpetch S, Yenjai C and Kukongviriyapan V: Derrischalcone suppresses cholangiocarcinoma cells through targeting ROS-mediated mitochondrial cell death, Akt/mTOR, and FAK pathways. Naunyn Schmiedebergs Arch Pharmacol 394: 1929-1940, 2021.
19. Nazim UM, Yin H and Park SY: Autophagy flux inhibition mediated by celastrol sensitized lung cancer cells to TRAIL-induced apoptosis via regulation of mitochondrial transmembrane potential and reactive oxygen species. Mol Med Rep 19: 984-993, 2019.
20. Nogales C, Mamdouh ZM, List M, Kiel C, Casas AI and Schmidt H: Network pharmacology: Curing causal mechanisms instead of treating symptoms. Trends Pharmacol Sci 43: 136-150, 2022.
21. Zhang P, Zhang D, Zhou W, Wang L, Wang B, Zhang T and Li S: Network pharmacology: Towards the artificial intelligence-based precision traditional Chinese medicine. Brief Bioinform 25: bbad518, 2023.
22. Zhao L, Zhang H, Li N, Chen J, Xu H, Wang Y and Liang Q: Network pharmacology, a promising approach to reveal the pharmacology mechanism of Chinese medicine formula. J Ethnopharmacol 309: 116306, 2023.
23. Livak KJ and Schmittgen TD: Analysis of relative gene expression data using real-time quantitative PCR and the 2(-Delta Delta C(T)) method. Methods 25: 402-408, 2001.
24. Esmat A, El-Demerdash E, El-Mesallamy H and Abdel-Naim AB: Toxicity and oxidative stress of acrylonitrile in rat primary glial cells: Preventive effects of N-acetylcysteine. Toxicol Lett 171: 111-118, 2007.
25. Du L, Empey PE, Ji J, Chao H, Kochanek PM, Bayır H and Clark RS: Probenecid and N-Acetylcysteine prevent loss of intracellular glutathione and inhibit neuronal death after mechanical stretch injury in vitro. J Neurotrauma 33: 1913-1917, 2016.
26. Strickson S, Campbell DG, Emmerich CH, Knebel A, Plater L, Ritorto MS, Shpiro N and Cohen P: The anti-inflammatory drug BAY 11-7082 suppresses the MyD88-dependent signalling network by targeting the ubiquitin system. Biochem J 451: 427-437, 2013.
27. Wilbur HC, Soares HP and Azad NS: Neoadjuvant and adjuvant therapy for biliary tract cancer: Advances and limitations. Hepatology 82: 1287-1302, 2025.
28. Wang JX, Zhang MX, Yu CH, Wang SJ and Zhang H: Targeting DNA damage: A natural product-based strategy for inhibiting cancer progression. J Ethnopharmacol 355: 120643, 2026.
29. Ma J, Zhang Y, Du J, Chen J, Sun J, Ma X, Zeng J and Efferth T: High-fat Diet-associated digestive cancers: Mechanisms, natural Product-based therapies, and drug development. Phytomedicine 150: 157574, 2026.
30. He Z, Wang Y, Han L, Hu Y and Cong X: The mechanism and application of traditional Chinese medicine extracts in the treatment of lung cancer and other lung-related diseases. Front Pharmacol 14: 1330518, 2023.
31. Ismail T, Kim Y, Lee H, Lee DS and Lee HS: Interplay between mitochondrial peroxiredoxins and ROS in cancer development and progression. Int J Mol Sci 20: 4407, 2019.
32. Li J, Lim JYS, Eu JQ, Chan AKMH, Goh BC, Wang L and Wong AL: Reactive oxygen species modulation in the current landscape of anticancer therapies. Antioxid Redox Signal 41: 322-341, 2024.
33. Ebrahimi SO, Reiisi S and Shareef S: miRNAs, oxidative stress, and cancer: A comprehensive and updated review. J Cell Physiol 235: 8812-8825, 2020.
34. Imran M, Saeed F, Gilani SA, Shariati MA, Imran A, Afzaal M, Atif M, Tufail T and Anjum FM: Fisetin: An anticancer perspective. Food Sci Nutr 9: 3-16, 2020.
35. Huang M and Xin W: Matrine inhibiting pancreatic cells epithelial-mesenchymal transition and invasion through ROS/NF-κB/MMPs pathway. Life Sci 192: 55-61, 2018.
36. Lin K, Zhang Y, Shen Y, Xu Y, Huang M and Liu X: Hydrogen sulfide can scavenge free radicals to improve spinal cord injury by inhibiting the p38MAPK/mTOR/NF-κB signaling pathway. Neuromolecular Med 26: 26, 2024.
37. Montal R, Sia D, Montironi C, Leow WQ, Esteban-Fabró R, Pinyol R, Torres-Martin M, Bassaganyas L, Moeini A, Peix J, *et al*: Molecular classification and therapeutic targets in extrahepatic cholangiocarcinoma. J Hepatol 73: 315-327, 2020.
38. Pan S, Hu Y, Hu M, Xu Y, Chen M, Du C, Cui J, Zheng P, Lai J, Zhang Y, *et al*: S100A8 facilitates cholangiocarcinoma metastasis via upregulation of VEGF through TLR4/NF-κB pathway activation. Int J Oncol 56: 101-112, 2020.